Contents lists available at ScienceDirect

Computational and Structural Biotechnology Journal

Research article

A hypoxia-derived gene signature to suggest cisplatin-based therapeutic responses in patients with cervical cancer

Jin Fang [a,1], Ying Wang [a,1], Chen Li [a,b,1], Weixiao Liu [a], Wannan Wang [a,b], Xuewei Wu [a], Yang Wang [b,*], Shuixing Zhang [a,b,**], Jing Zhang [a,b,**]

[a] *Department of Radiology, The First Affiliated Hospital of Jinan University, Guangzhou 510613, China*
[b] *MOE Key Laboratory of Tumor Molecular Biology, The First Affiliated Hospital of Jinan University, Guangzhou 510613, China*

A R T I C L E I N F O

A B S T R A C T

Cervical cancer remains a significant global public health concern, often exhibits cisplatin resistance in clinical settings. Hypoxia, a characteristic of cervical cancer, substantially contributes to cisplatin resistance. To evaluate the therapeutic efficacy of cisplatin in patients with cervical cancer and to identify potential effective drugs against cisplatin resistance, we established a hypoxia-inducible factor-1 (HIF-1)-related risk score (HRRS) model using clinical data from patients treated with cisplatin. Cox and LASSO regression analyses were used to stratify patient risks and prognosis. Through qRT-PCR, we validated nine potential prognostic HIF-1 genes that successfully predict cisplatin responsiveness in patients and cell lines. Subsequently, we identified fostamatinib, an FDA-approved spleen tyrosine kinase inhibitor, as a promising drug for targeting the HRRS-high group. We observed a positive correlation between the IC50 values of fostamatinib and HRRS in cervical cancer cell lines. Moreover, fostamatinib exhibited potent anticancer effects on high HRRS groups *in vitro* and *in vivo*. In summary, we developed a hypoxia-related gene signature that suggests cisplatin response prediction in cervical cancer and identified fostamatinib as a potential novel treatment approach for resistant cases.

1. Introduction

Cervical cancer ranks fourth throughout the world in incidence and remains a leading cause of cancer-related mortality in women worldwide [1,2]. According to the National Comprehensive Cancer Network guidelines, early-stage cervical cancer is typically treated with radical hysterectomy and lymph node dissection [3]. Locally advanced cervical cancer is conventionally managed with adjuvant concurrent chemoradiotherapy [4]. Cisplatin-based chemotherapy constitutes the cornerstone of treatment for patients with recurrent or metastatic cervical cancer, as it insignificantly reduces the risk of mortality by approximately 30–50 % [4]. However, a significant proportion of patients eventually develop cisplatin resistance, thus leading to therapy failure and increased mortality rates [5]. Therefore, there is an imperative need to identify more accurate predictors for cervical cancer to identify patients who stand to benefit from cisplatin-based chemotherapy.

Hypoxia, a characteristic feature of solid tumors, contributes to cancer resistance against various treatment modalities, such as radiotherapy, conventional chemotherapy, immunotherapy, and targeted therapy [6,7]. Specifically, in cisplatin-resistant cancers, hypoxia fosters aberrant pathological manifestations, such as disrupted vasculature, decreased p53 expression and DNA mismatch repair, increased cell cycle arrest, low intracellular pH, and epithelial to mesenchymal transition (EMT) [8,9]. These alterations establish a conducive environment for tumor cells to evade the therapeutic effects of cisplatin [10,11]. As the principal mediator of the hypoxic response, hypoxia-inducible factor-1 (HIF-1) disrupts the transcription of essential target proteins such as VEGF, IL-6, and survivin, thereby hindering drug-induced apoptosis [12]. Although several studies have focused on developing hypoxia-based approaches for predicting tumor grade and prognosis [13–15], there is currently no established hypoxia-related gene signature for screening patients with cervical cancer to identify those patients who are likely to benefit from cisplatin therapy and to predict its

---

* Correspondence to: MOE Key Laboratory of Tumor Molecular Biology, Jinan University, Guangzhou 510632, China.
** Corresponding authors at: Department of Radiology, The First Affiliated Hospital of Jinan University, Guangzhou 510613, China.
E-mail addresses: wangyang0507@jnu.edu.cn (Y. Wang), zsx7515@jnu.edu.cn (S. Zhang), zj6410@jnu.edu.cn (J. Zhang).
[1] These authors contributed equally to this work.

effectiveness.

In this study, we established a prognostic model termed the HIF-1-related risk score (HRRS) for patients with cervical cancer who received cisplatin treatment by using data from a cervical cancer cohort. The ability of HRRS to suggest cisplatin responses was evaluated across various cervical cancer cell lines. Additionally, gene–drug association analysis was performed based on risk characteristics, which identified fostamatinib (an FDA-approved drug) as a potential candidate for treating patients with HRRS-high. Both *in vivo* and *in vitro* experiments corroborated the advantageous effects of fostamatinib in combating cisplatin-resistant cervical cancer cells. In summary, our HRRS model demonstrates promise in suggesting the cisplatin therapy response in patients with cervical cancer and presents an avenue for personalized cancer management.

2. Materials and methods

2.1. Reagents and chemicals

Cisplatin ($\geq$ 98 % purity), isoflurane and dimethyl sulfoxide (DMSO) were acquired from Chinese Sigma Reagent Network (Shanghai, China), and fostamatinib ($\geq$ 98 % purity) was purchased from GlpBio Chinese Station (Shanghai, China). Dulbecco's modified Eagle's medium (DMEM), fetal bovine serum (FBS) and penicillin—streptomycin (P/S) were obtained from Gibco (Waltham, MA, USA).

2.2. Cell lines and culture conditions

Human cervical cancer cell lines including HeLa, Siha, C33A and Caski, were obtained from the American Type Culture Collection (ATCC, Manassas, VA, USA). All cell lines were maintained in complete DMEM supplemented with 10 % FBS and 1 % P/S at 37 °C with 5 % CO_2.

2.3. Data collection

The clinical (Supplementary Table S1) and mRNA (Supplementary Table S2) expression information of cervical cancer patients (n = 115) treated with cisplatin from The Cancer Genome Atlas (TCGA) was downloaded through the online tool Sangerbox (http://sangerbox.com/; accessed on April 25th 2022). HIF-1 related genes were downloaded from the Kyoto Encyclopedia of Genes and Genomes database (KEGG, https://www.genome.jp/kegg/; accessed on April 25th 2022). Magnetic resonance imaging (MRI) (Supplementary Table S3) data were collected from The Cancer Imaging Archive (TCIA, https://wiki.cancerimaging archive.net/pages/viewpage.action?pageId=19039396; accessed on October 7th 2022). An expression matrix file (GSE113005, Supplementary Table S4) of cancer cells treated with fostamatinib or vehicle control [16] was downloaded from the Gene Expression Omnibus (GEO) (http://www.ncbi.nlm.nih.gov/geo/; accessed on December 3rd 2023).

2.4. MRI image segmentation

The MRI images were opened using ITK-SNAP v3.8.0 software, and the lesion was distinguished from the surrounding normal tissue on sagittal (SAG) and axial (AX) T2WI images according to the signal difference. Subsequently, to assess the size, shape, and characteristics of the cervical cancer, the region of interest (ROI) area of the lesion was obtained by a radiologist (Jin Fang) with a decade-long experience in interpreting MRI images for cervical cancer. The results were then independently validated by two other radiologists (Shuixing Zhang and Ying Wang) who have 20 years and 5 years of experience in interpreting MRI images respectively, in order to minimize potential bias.

2.5. HIF-1 related gene signature generation

To identify prognostic genes related to cisplatin-treated cervical

cancer, we used the R software package "survival" [17] to integrate survival time, survival status, and gene expression data, and evaluated the prognostic significance of each gene using the single-factor Cox analysis [18]. With log-rank test *p* value < 0.05, we identified 2348 prognostic genes for cervical cancer (Supplementary Table S5). The genes overlapping between cervical cancer prognostic genes and HIF-1 related genes were selected for LASSO Cox regression analysis by using the "Glmnet" R package [19,20]. With the tenfold cross-validation method, we screened out the most candidate genes. Afterwards, we used the expression levels and corresponding LASSO Cox coefficients to calculate the HIF-1 related risk score (HRRS) for each patient. The formula was as follows: $HRRS = \sum i \, Coefficient(mRNAi) \times Expression(mRNAi)$. Based on the median risk score, the patients were categorized into high-risk and low-risk groups, and the relationships between HRRS and gene expression levels, survival time and survival status were analyzed. Similarly, two previously reported seven-gene signature (ACSL1, ALDOA, FOXK2, GPI, MDH1B, MDH2 and MTHFD1) and the six-gene signature (HSPA5, ANGPTL4, PFKM, GOT1, IER3 and PFKFB4) were calculated according to their mentioned corresponding coefficients [21,22] and the gene expression levels in cisplatin-treated patients (TCGA cohort). Patients were stratified into high-risk and low-risk groups according to the median level of the six-gene signature or seven-gene signature for following survival analysis. Furthermore, the Kaplan-Meier (K—M) survival analysis was conducted by using the R package "survivalROC", whereas receiver operating characteristic (ROC) curve analysis and area under the receiver operating characteristic curve (AUC) were performed using the R packages "survConcordance" and "survivalROC".

2.6. Enrichment analysis

Gene Ontology (GO) [23–25], Kyoto Encyclopedia of Genes and Genomes (KEGG) [26] and gene set enrichment analyses (GSEA) [27] analysis were conducted, as has been previously described [28]. In brief, we utilized the R package "clusterProfiler v4.4.4" [24,25] for GO and KEGG analyses, and GSEA Software v3.0 for GSEA analyses. GSEA defines significance as having a normalized enrichment score (NES) with an absolute value greater than or equal to 1, a nominal *p* value (NP) less than 0.05, and a *p* value after Benjamin-Hochberg adjustment, which indicates a false discovery rate (FDR) less than 0.25.

2.7. Identification of differentially expressed genes (DEGs)

The identification of DEGs between the high- and low-risk groups was performed using the R package "t.test" with the criteria of a fold change (FC) $\geq$ 1.5 and *p* < 0.05. The expression profiles of the top 50 DEGs were visualized through heatmap plots.

2.8. Gene–drug association analysis

The WEB-based gene set analysis toolkit (WebGestalt, http://www.webgestalt.org/; accessed on May 5th 2022) was used to predict the potential drugs associated with upregulated genes in the high HRRS-group. Based on the given parameters (organism: *Homo sapiens*; method: overrepresentation analysis; functional database: DrugBank; minimum number of genes for a category: 5; maximum number of genes for a category: 2000; multiple test adjustment: BH; significance level: 10), fostamatinib was identified as the preferred drug choice. The interaction network between fostamatinib and associated genes was generated by using a web-based application named STITCH (http://stitch.embl.de/; accessed on 5 May 2022).

2.9. qRT—PCR

qRT—PCR was performed as previously described [29] with minor modifications. Briefly, the total RNA extraction was performed out using

TRIzol (Invitrogen, CA, USA), and cDNA synthesis was performed using the PrimeScriptTM RT Reagent Kit with gDNA Eraser (Takara Biomedical Technology, Beijing, China). Real-time PCR was then utilized to measure the gene expression levels of *EGLN1, AKTIP, ANGPT2, SERPINE1, EGFR, PRKCB, CAMK2N2, IFNG*, and *PIK3R2* following the instructions provided by the manufacturer. The experiment was conducted in triplicate using the Applied Biosystems Step One Plus System 2.2.3 (Thermo Fisher Scientific) with SYBR Green PCR Master Mix (Bio-Rad, Hercules, CA, USA). The cycle threshold (CT) values of each sample were utilized to analyze the PCR-derived data. The utilized primers for qRT—PCR are listed in Table 1.

2.10. Cell viability assay

Cervical cancer cells were cultured in 96-well plates for 24 h before being exposed to various drug concentrations for an additional 24 h. The viability of these cells was assessed using a CCK-8 assay (Topscience, Shanghai, China), as has been previously described [30]. The IC50s were calculated by GraphPad Prism 9.

2.11. Colony formation assay

To analyze the ability of cells to survive long-term drug treatment, cells were seeded into 6-well plates at a density of 2000 cells per well. These cells were cultured for 4 days and then treated with different concentrations of fostamatinib for another 10 days. After two washes with PBS, the plates were fixed with methanol for 10 min at room temperature and stained them with 1 % crystal violet for another 10 min. The colonies were counted using ImageJ software v 1.44I.

2.12. Animal experiments and treatments

Female Athymic Nu/Nu mice (aged 4–5 weeks) were acquired from Vitonlihua (Beijing, China) and housed in accordance with the Institutional Animal Care and Use Laboratory Animal Center at Jinan University in Guangzhou, China (Approval No. IACUC-20210915–03). To induce subcutaneous implantation of cervical cancer tumors, HeLa cells were injected into the groin of mice. The cells were suspended in 200 μL of PBS at a concentration of 5×10^6 cells per mouse. Once the average tumor volume reached 200–300 mm^3, the mice were randomly divided into three different experimental groups (n = 5 per group): the control group, which received only the vehicle; the treatment Group 1, which received 40 mg/kg fostamatinib intraperitoneally once daily; and treatment Group 2, which received 80 mg/kg fostamatinib

Table 1
Primer sequences for qRT-PCR.

Primer	Sequences (5'->3')
EGLN1 *Forward*	GACGACCTGATACGCCACT
EGLN1 *Reverse*	ACATGACGTACATAACCCGTTC
AKTIP *Forward*	GCAGCCATCTTATCGCTCT
AKTIP *Reverse*	AACTGTAAACTTAAATACGCCAT
ANGPT2 *Forward*	TAAGCAGCATCAGCCAACCA
ANGPT2 *Reverse*	GCCTCCTGTTAGCATTTGTGA
SERPINE1 *Forward*	TCATATCCTTGCCCTTGAGT
SERPINE1 *Reverse*	CCACAAAGAAACACTAGGAGC
EGFR *Forward*	CTGGTCTGCCGCAAATTCCG
EGFR *Reverse*	GGACACTTCTTCACGCAGGT
PRKCB *Forward*	ACTTGACAACGTGATGCTCGAT
PRKCB *Reverse*	AGAATGTCTTGGTTGTCACCCC
CAMK2N2 *Forward*	GCCTCAGCCTCTTTCTAAGGGAC
CAMK2N2 *Reverse*	GCCTCAACACCCATCCTATCTGC
IFNG *Forward*	GATTACAAGGCTTTATCTCA
IFNG *Reverse*	CAGGCATATTTTCAAACCG
PIK3R2 *Forward*	CCCGGCAGAAGAAAATCAACGA
PIK3R2 *Reverse*	TTGATCTTGCCCACGTACCAA
GADPH *Forward*	TCTGACTTCAACAGCGACACC
GADPH *Reverse*	CTGTTGCTGTAGCCAAATTCGTT

intraperitoneally once daily. The relative tumor volume was calculated using the following formula: Volume (mm^3) = (length $\times$ width^2) $\times$ 0.5. At the end of the experiment, all naked rodents were euthanized and their tumors were weighed. After the mice were sacrificed, blood was collected to determine biochemical and hematological parameters; additionally, tumor tissues were collected for immunohistochemical analysis with Ki-67 and TUNEL assays, and organs (heart, liver, spleen, lung, and kidney) were collected for hematoxylin and eosin (H&E) staining.

2.13. High-field (9.4 T) MRI

The MRI images of the mice were obtained by using a BioSpec 94/30 small animal 9.4 T MRI system (Bruker BioSpin, Ettlingen, Germany) equipped with ParaVision software v6.0.1. Image acquisition was performed using a rat body quadrature volume coil with an inner diameter of 86 mm (Bruker BioSpin, Ettlingen, Germany). Each animal was placed in a prone position on a rat cradle. A self-selected echo sequence (SE) was utilized for imaging. T1-weighted images were acquired with the following parameters: echo time (TE): 3 ms, repetition time (TR): 3100 ms, average: 4, slice thickness: 1 mm, matrix size: 256 $\times$ 256, field of view (FOV): 35 $\times$ 35 cm^2, and acquisition time (TA): 179 s). T2-weighted images were obtained with the following parameters: TE: 20 ms, TR: 2000 ms, average: 3, thickness: 1 mm, matrix size: 256 $\times$ 256, and FOV: 35 $\times$ 35 cm^2. During MRI acquisition, the mice were anesthetized with isoflurane (2–3 % maintenance anesthesia concentration), and their temperature, heart rate, and respiration were monitored.

2.14. Statistical analysis

Statistical analysis was performed using GraphPad Prism 8.0 software. The data are represented as the mean $\pm$ the standard deviation (SD). For all comparisons between the control and treatment groups, p values were calculated using Student's t tests. For statistical significance, * $p < 0.05$, * * $p < 0.01$, and * ** $p < 0.001$.

3. Results

3.1. Establishment of a hypoxia-related prognostic signature for cisplatin-treated patients with cervical cancer

Given that hypoxia is identified as the primary contributor to cisplatin resistance [7], we downloaded 93 genes associated with the HIF-1 signaling pathway (HIF-1 is a core transcription factor in hypoxia) from the KEGG database to construct a feasible hypoxia-associated prognostic model for assessing survival risk among cisplatin-treated patients with cervical cancer. Subsequently, we intersected the HIF-1-related genes with 2348 cervical cancer prognostic genes (Supplementary Table S5; log-rank < 0.05), which were identified through single-factor Cox analysis, thus yielding 19 prognosis-related genes linked to HIF-1 (Fig. 1A; Supplementary Table S6). LASSO regression analysis was then applied to these 19 genes to identify the prognostic genes (Fig. 1B). By employing tenfold cross-validation to mitigate the overfitting, with an optimal λ of 0.05, we identified a total of nine genes (*EGLN1, AKTIP, ANGPT2, SERPINE1, EGFR, PRKCB, CAMK2N2, IFNG*, and *PIK3R2*) (Fig. 1C). Subsequently, on the basis of the expression levels of these nine genes along with their corresponding LASSO Cox coefficients, we established the HRRS as follows: HRRS = (0.65 $\times$ expression of *EGLN1*) + (0.59 $\times$ expression of *AKTIP*) + (0.23 $\times$ expression of *ANGPT2*) + (0.14 $\times$ expression of *SERPINE1*) + (0.03 $\times$ expression of *EGFR*) + (−0.11 $\times$ expression of *PRKCB*) + (−0.20 $\times$ expression of *CAMK2N2*) + (−0.46 $\times$ expression of *IFNG*) + (−0.51 $\times$ expression of *PIK3R2*). The nine genes displayed a close protein-protein interaction network (Fig. 1D) and were functionally linked to angiogenesis regulation, protein import, the Rap1 signaling pathway, the Ras
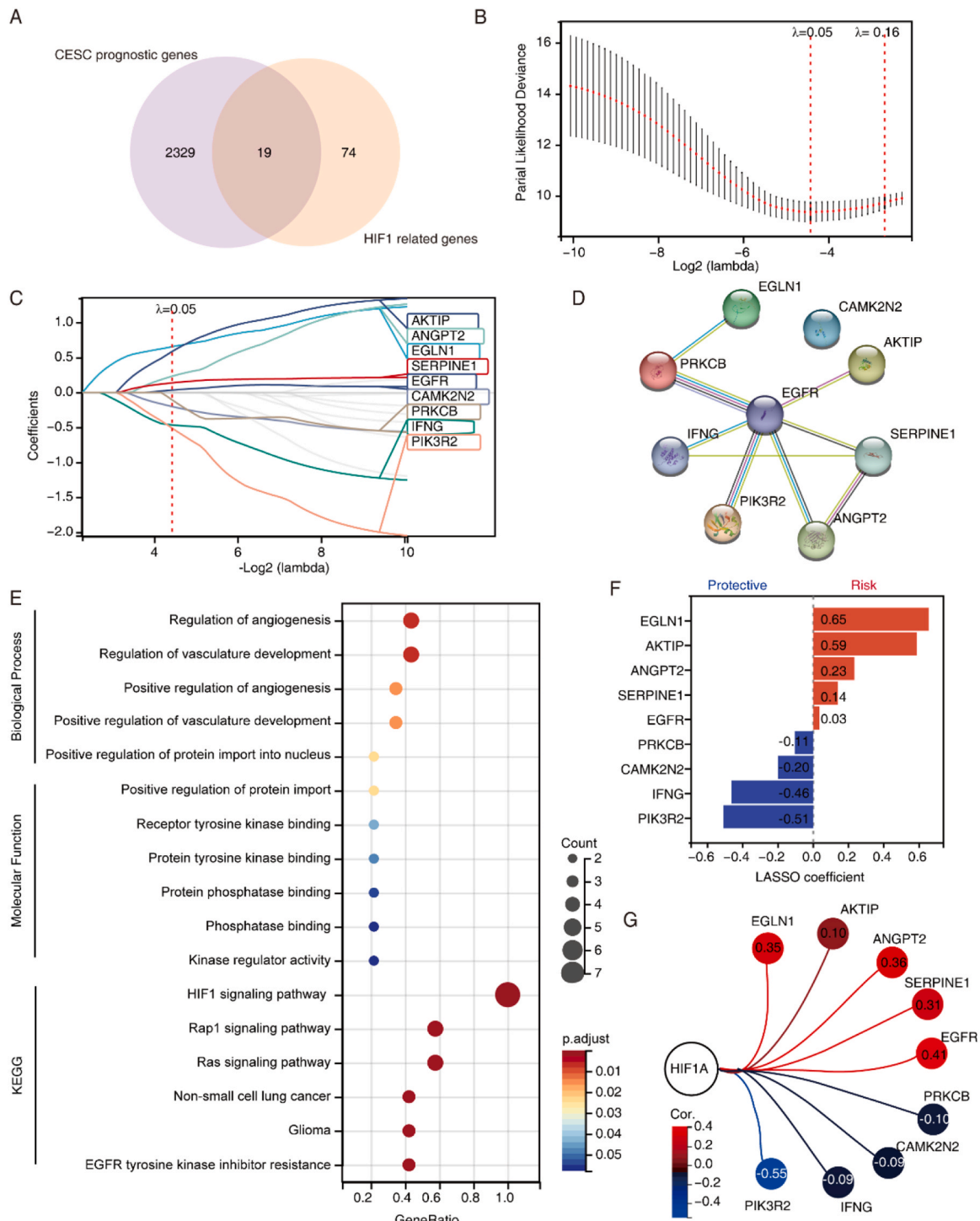
Fig. 1. Construction of the prognostic HIF-1-related gene signature based on the TCGA cohort. (A) The intersection of HIF-1-related genes and cervical cancer prognostic genes is visualized in a Venn diagram. (B, C) LASSO regression analysis of the 19 overlapping genes. (D) A PPI network of the nine key HIF-1-related genes. (E) GO analysis (biological processes and molecular functions) and KEGG pathway enrichment analysis of the nine key HIF-1-related genes. (F) LASSO coefficients for the nine key HIF-1-related genes. (G) The correlation between the mRNA expression levels of HIF-1 and those of the nine key HIF-1-related genes.

signaling pathway, EGFR tyrosine kinase inhibitor resistance, and the HIF-1 signaling pathway (Fig. 1E). Among the nine genes, *EGLN1*, *AKTIP, ANGPT2, SERPINE1* and *EGFR* were identified as risk factors that were positively correlated with *HIF-1* expression, whereas *PRKCB*, *CAMK2N2, IFNG,* and *PIK3R2* were identified as protective variables that were negatively correlated with *HIF-1* (Fig. 1F, G).

3.2. HRRS serves as a potential indicator of poor prognosis and malignancy

We stratified cisplatin-treated patients with cervical cancer into high- and low-risk groups based on the median value of HRRS (Supplementary Table S7) and observed elevated expression levels of the five risk-associated genes in the high-risk group compared to the low-risk group, whereas the four protective genes exhibited the opposite trend.

The differences in the expression of these nine genes between the high- and low-risk groups were significant, as indicated by the *p* values (Fig. 2A). An expression heatmap elucidated the detailed relationship between the expression of the nine genes and HRRS. As the HRRS increased, patients with cervical cancer had shorter survival times and increased mortality, as indicated by more patients (red dots) in the group with high-risk scores (right side of the dashed line), in which the expression of protective genes (*PRKCB, CAMK2N2, IFNG,* and *PIK3R2*) decreased (Fig. 2B). Moreover, a greater proportion of stage IV cases was correlative with HRRS-high (Fig. S1A). Other clinical characteristics, such as age, tumor type (T), lymph node status (N), metastasis status (M) and histologic grade, were not significantly associated with the HRRS (Fig. S1A). Kaplan–Meier analysis of the HRRS demonstrated that a higher HRRS (high-risk group) was significantly associated with poorer prognosis in cisplatin-treated patients (HR = 6.17, $p = 1.6e-6$; Fig. 2C). The predictive performance of the HRRS was assessed by using 1-, 3-, and 5-year ROC curves, and the average AUC values for 1-, 3-, and 5-year

prognosis prediction in cisplatin-treated patients with cervical cancer reached 0.90, 0.85 and 0.87, respectively (Fig. 2D).

We also conducted two previously reported six-gene signature [22] and seven-gene signature [21] used in cervical cancer, to compare their performance on cisplatin-treated patients from TCGA cohort with our HRRS model. According to result of six-gene signature, cisplatin-treated patients with high-risk group displayed lower survival (HR = 2.85, $p = 3.8e-3$) than low-risk group, with AUC values for 1-, 3-, and 5-year prognosis prediction in cisplatin-treated cervical cancer patients reached 0.74, 0.70 and 0.69, respectively (Fig. S2A-C). For the performance of seven-gene signature, cisplatin-treated patients with high-risk group displayed no significant difference in survival rate with low-risk group (HR = 0.97, $p = 0.93$), and the AUC values for 1-, 3-, and 5-year prognosis prediction in cisplatin-treated patients with cervical cancer reached 0.54, 0.52 and 0.52, respectively (Fig. S2D-F), suggesting the performance of our HRRS to assess the cisplatin response of cervical cancer patients is better than two reported multigene models.
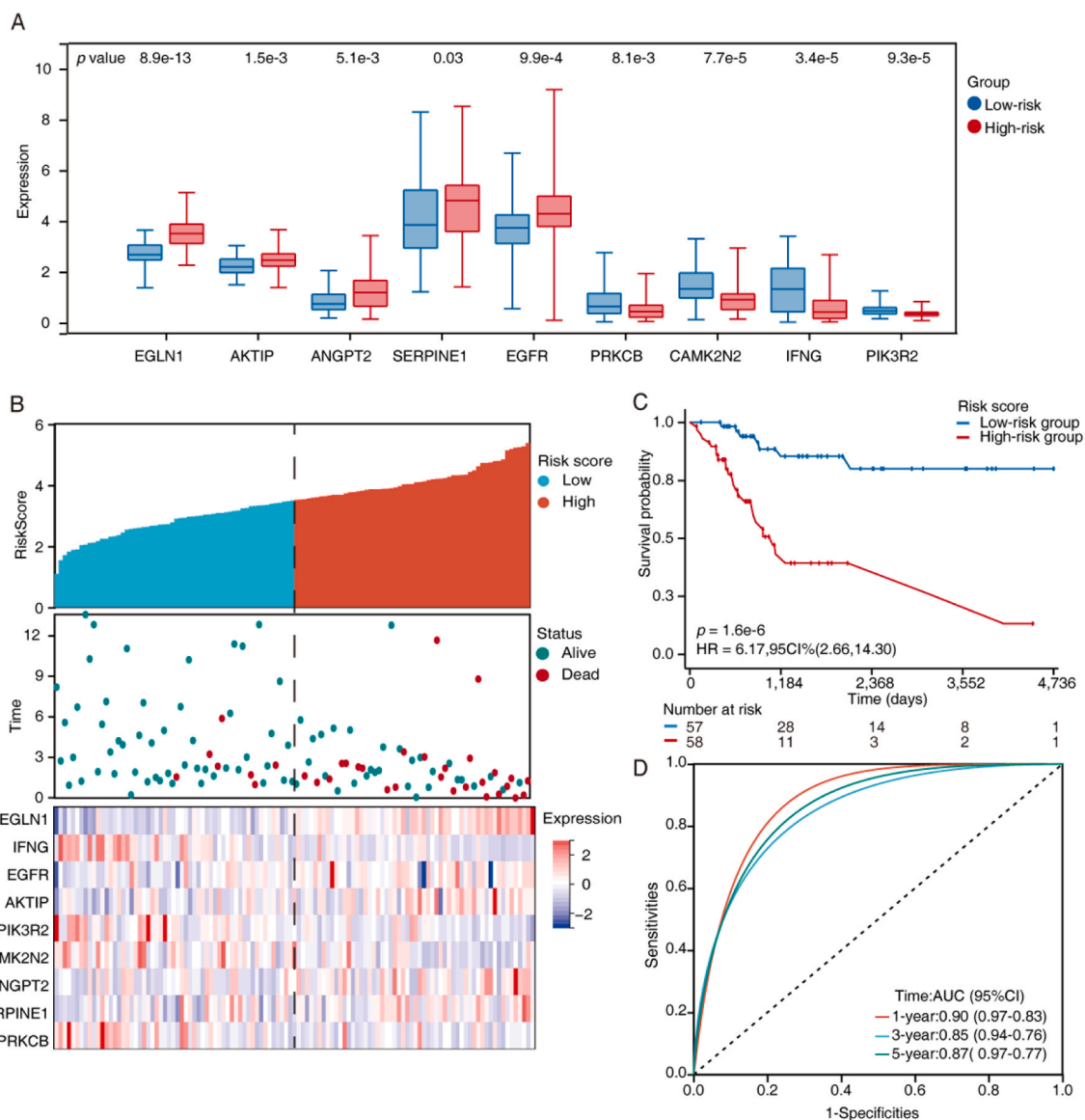

Fig. 2. Assessment of the prognostic HIF-1-related gene signature. (A) Boxplots were generated to compare the expression levels of the nine key HIF-1-related genes between the high- and low-risk groups. (B) A comparison between the risk scores and survival statuses of cisplatin-treated patients with cervical cancer. The corresponding mRNA expression Z scores of the nine genes are depicted using a heatmap. The dashed line stratifies all of the patients into high- and low-risk groups based on the median value of HRRS. The right side of the dashed line represents patients with high-risk score, which is associated with more deaths (red dots). (C) Survival curves of cisplatin-treated patients categorized as high or low risk in the TCGA cervical cancer cohort. (D) ROC plots and AUC scores at 1, 3, and 5 years were generated to assess the overall survival prediction capability of the HRRS.

Furthermore, we developed a nomogram based on the HRRS and clinicopathological variables, including stage and grade, to quantify the risk and survival probability for individual cisplatin-treated patients. The nomogram demonstrated that only the statistical outcomes of the HRRS exhibited significant differences, thus justifying their inclusion in the model construction (Fig. S1B). Calibration analysis demonstrated that the nomogram's prediction lines for 3- and 5-year survival probabilities closely approximated the ideal performance (45-degree line) (Fig. S1C). Compared with other features, the nomogram exhibited a similar predictive capacity to HRRS for survival, with an average AUC of approximately 0.9, which was markedly superior to that of clinical stage and histologic grade (Fig. S1D). These results suggest that the HRRS could serve as a potential individual factor for quantifying risk and survival probability in cisplatin-treated patients.

We subsequently analyzed the clinical significance of the high- and low-HHRS groups in 17 patients with cervical cancer who had available preoperative whole-volume tumor MRI images, transcriptomic data, and clinical information. Patients with high HRRS had a higher proportion of T-stage 4, stage IVA- IVB, and mortality outcomes compared to those with low HRRS. In addition, individuals classified as unclassified (grade X, T-stage X) were more likely to be associated with the high-risk group (Fig. 3A; Supplementary Table S8). The transcriptomic profiles of the nine genes in the two HRRS subtypes were depicted in a heatmap (Fig. 3A). Despite the small sample size of 17 patients, it remains evident that five risk-associated genes (*EGLN1*, *AKTIP*, *ANGPT2*, *SERPINE1*, and *EGFR*) were upregulated in the high-HRRS group, whereas protective genes (*PRKCB*, *CAMK2N2*, *IFNG*, and *PIK3R2*) were enriched in the low-risk group. In the ROI in the MRI images, it is observable that cases in the
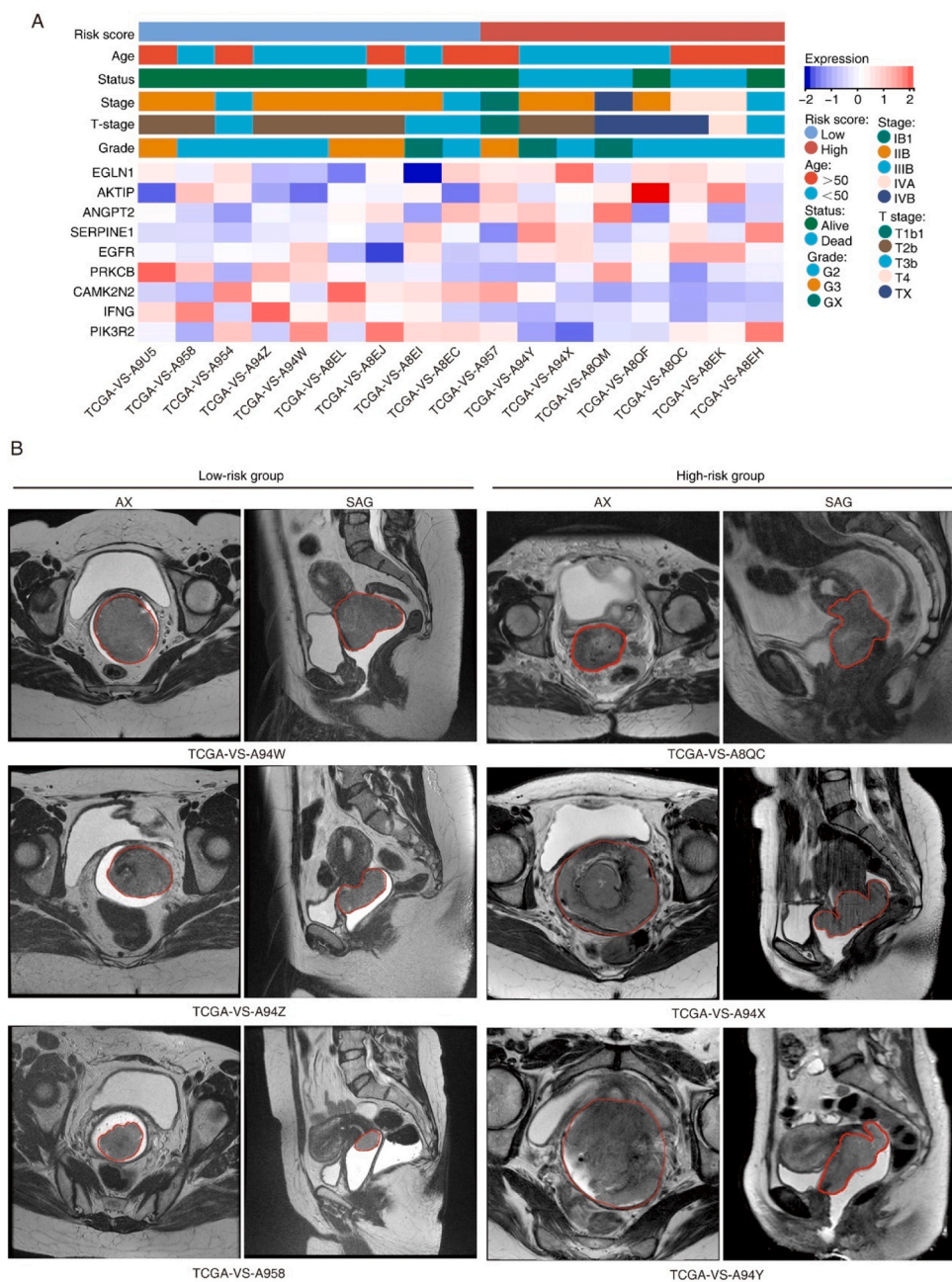

Fig. 3. Clinical significance of the high- and low-HRRS groups. (A) Unsupervised clustering of all HRRS-related genes in 17 patients with cervical cancer with available preoperative whole-volume tumor MRI images. Patient annotations included risk score, age, status, stage, tumor stage, and histologic grade. (B) Representative MRI images of patients from the low- and high-risk groups, displaying axial and sagittal T2W images for each patient with the ROI delineated in red.

low-risk group displayed regular shapes, smooth margins, and distinct boundaries, whereas those in the high-risk group had large, irregular, heterogeneous masses that breached the cervical stroma and exhibited parauterine infiltration (Fig. 3B). Notably, five patients, including TCGA-VS-A958, TCGA-VS-A94Z, TCGA-VS-A94W, TCGA-VS-A94Y, and TCGA-VS-A94X, consistently presented with clinical stage IIB. However, our HRRS was able to categorize patients into high- and low-risk groups, thus aligning with the MRI results. These results indicate the good predictive performance of the nine-gene signature in distinguishing differences in cervical cancer-grade malignancy and outcomes.

3.3. The HRRS is a promising predictor of cisplatin resistance

Given the ability of the HRRS to suggest the clinical outcomes of cervical cancer patients who receive cisplatin treatment, we conducted additional experiments to examine whether this gene signature could serve as an indicator for cisplatin resistance *in vitro*. To achieve this, we performed qRT—PCR to quantify the mRNA expression levels of *EGLN1*, *AKTIP*, *ANGPT2*, *SERPINE1*, *EGFR*, *PRKCB*, *CAMK2N2*, *IFNG*, and *PIK3R2* in different cervical cancer cell lines (Fig. 4A). These cell lines encompassed diverse histological subtypes, including cervical squamous cell carcinoma (SiHa and Caski) and cervical adenocarcinoma (HeLa and C33A), thereby facilitating cross-validation of our findings to ensure the potential of HRRS. By using HeLa cells as a control, we observed the highest expression of most genes in Caski, whereas the expression levels of the five risk-associated genes were lowest in C33A (Supplementary Table S9). These results indicate significant variations in the expression levels of the nine genes among the four cell lines. Additionally, HRRS values were calculated for each cell line based on the qRT—PCR assays, which yielded values of 0.36 for HeLa cells, − 1.14 for SiHa cells, − 1.84 for C33A cells, and − 2.19 for Caski cells (Fig. 4B). To determine the correlation between the HRRS of the four cell lines and their response to cisplatin, we evaluated the sensitivity of each cell line to cisplatin by treating them with increasing concentrations of cisplatin (0–50 μM) over a 24-h period. The IC50 values for cisplatin in HeLa, SiHa, C33A, and Caski cells were determined to be 32.18 ± 3.65, 26.43 ± 1.55, 1.12 ± 0.35, and 4.93 ± 0.57 μM, respectively (Fig. 4C). Through correlation analysis, we observed a positive correlation between the IC50 and HRRS in these cervical cancer cell lines ($R^2 = 0.79$; Fig. 4D). Specifically, cells with high HRRS, such as HeLa and SiHa cells, exhibited resistance to cisplatin, whereas those with low HRRS, namely C33A and Caski cells, demonstrated sensitivity to the drug. These results indicate that the signature may serve as a suggestive indicator of cisplatin resistance *in vitro*.

3.4. Differential biological behaviors of HRRS subtypes

To explore the underlying mechanisms contributing to differences in the degree of malignancy, cisplatin response, survival time, and survival status among the HRRS groups, we performed GSEA to identify hallmark gene sets associated with different risk groups. Using the criteria of | NES| ≥ 1, NP < 0.05, and FDR < 0.25, we identified 11 hallmark gene sets enriched in the cisplatin-treated TCGA cohort. Among these genes, eight hallmark gene sets were enriched in the high-risk group, encompassing genes related to TGF-β signaling, protein secretion, UV response, androgen response, cholesterol homeostasis, unfolded protein response, hypoxia, and glycolysis (Fig. 5A). Notably, these gene sets have been reported to be associated with chemoresistance and malignant tumor progression [10,31–37]. Moreover, genes highly expressed in the low-risk group were significantly enriched in allograft rejection, interferon-γ response, and interferon-α response (Fig. 5B). These results suggest that distinct patterns of hallmark gene sets in the two HRRS groups may partially explain the aforementioned disparities between high- and low-HRRS populations.

3.5. HRRS-based treatment strategy for cisplatin resistant patients

To identify potential drugs that could benefit patients with high HRRS, we employed Student's t test to discern DEGs between high- and low-risk groups. A total of 745 DEGs were identified, comprising 375 upregulated and 370 downregulated genes in the high-risk group (criteria: FC ≥ 1.5, p < 0.05; Fig. 6A; Supplementary Table S10). The expression levels of the top 50 DEGs were visualized *via* cluster analysis (Fig. 6B). The upregulated DEGs were primarily linked to EMT, KRAS signaling, apical junctions, inflammatory responses, androgen responses, spermatogenesis, peroxisomes, hedgehog signaling, and pancreatic β cells (Fig. 6C). Some of the enriched pathways, such as EMT [38], KRAS signaling [39], inflammatory response [40] and hedgehog signaling [41], are reported to link to cisplatin resistance. Notably, we found an upregulation of the androgen response pathway in patients with high HRRS. Although emerging evidence suggests a role for androgen receptor activation in cervical cancer progression [42,43], additional studies are necessary to investigate the complex interplay between the androgen response and cisplatin resistance in cervical cancer. Conversely, downregulated DEGs were associated with pathways such as cell cycle-related pathways and apoptosis, presenting potential therapeutic avenues for cancer (Fig. 6D). Subsequently, we employed the WebGestalt web-based tool to explore drug–gene interactions and found that fostamatinib exhibited the most significant association with the upregulated genes (Fig. 6E). Thereafter, we constructed a fostamatinib-gene interaction network using the STITCH database. Fostamatinib interacted with EMT-related genes, including *EGFR*, *RPS6KA3*, *STAT3*, *HIPK2*, *SMAD2*, *SMAD7*, *BMPR2*, *ACVR1*, *TGFBR1*, *SHC1*, and *GRB2*, forming a tightly interconnected network (Fig. 6F). Fostamatinib, an FDA-approved specific spleen tyrosine kinase (SYK) inhibitor, has demonstrated significant efficacy in treating chronic lymphocytic leukemia [44] and pancreatic ductal adenocarcinoma [45]. Currently, research on fostamatinib's application in cervical cancer is limited; herein, our study identified fostamatinib as a potential therapeutic option for patients with cisplatin-resistant cervical cancer. To establish a clear relationship between fostamatinib and high-HRRS, we comprehensively analyzed the changes in the expression of DEGs between the high- and low-HRRS groups following fostamatinib treatment. We overlapped the upregulated and downregulated genes in the high-HRRS group with the 16,311 genes in an available gene expression dataset GSE113005, respectively (Table S11). Analysis of the gene expression alterations induced by fostamatinib in these overlapping genes revealed that the expression level of upregulated DEGs was predominantly downregulated (Fig. S3A), whereas the expression level of downregulated DEGs was mostly upregulated (Fig. S3B). These results indicate that fostamatinib may inhibit cisplatin-resistant cervical cancer by systematically altering the expression levels of DEGs between high- and low-HRRS groups.

3.6. Fostamatinib provides therapeutic efficacy against cisplatin-resistant cervical cancer cells in vitro and in vivo

To validate the anticancer effect of fostamatinib in cisplatin-resistant cervical cancer cells, we selected two relatively cisplatin-resistant cell lines (HeLa and SiHa cells) for subsequent *in vitro* experiments. Initially, both HeLa and SiHa cells were treated with increasing concentrations of fostamatinib (0–20 μM) for 24 h, and cell viability was determined by using a CCK-8 assay. As shown in Fig. 7A, fostamatinib exhibited a dose-dependent inhibition of cell viability in both HeLa and SiHa cells, with IC50 values of 6.96 ± 1.10 μM and 13.55 ± 0.72 μM, respectively. Fostamatinib-treated HeLa and SiHa cells exhibited significant cell shrinkage and diminished cellular adhesion (Fig. 7B). Moreover, we performed colony formation assay to examine the inhibitory effects of fostamatinib on the growth of cervical cancer cells. As shown in Fig. 7C, the colony formation of HeLa and SiHa cells was significantly inhibited by fostamatinib in a dose-dependent manner. Conversely, the cisplatin-
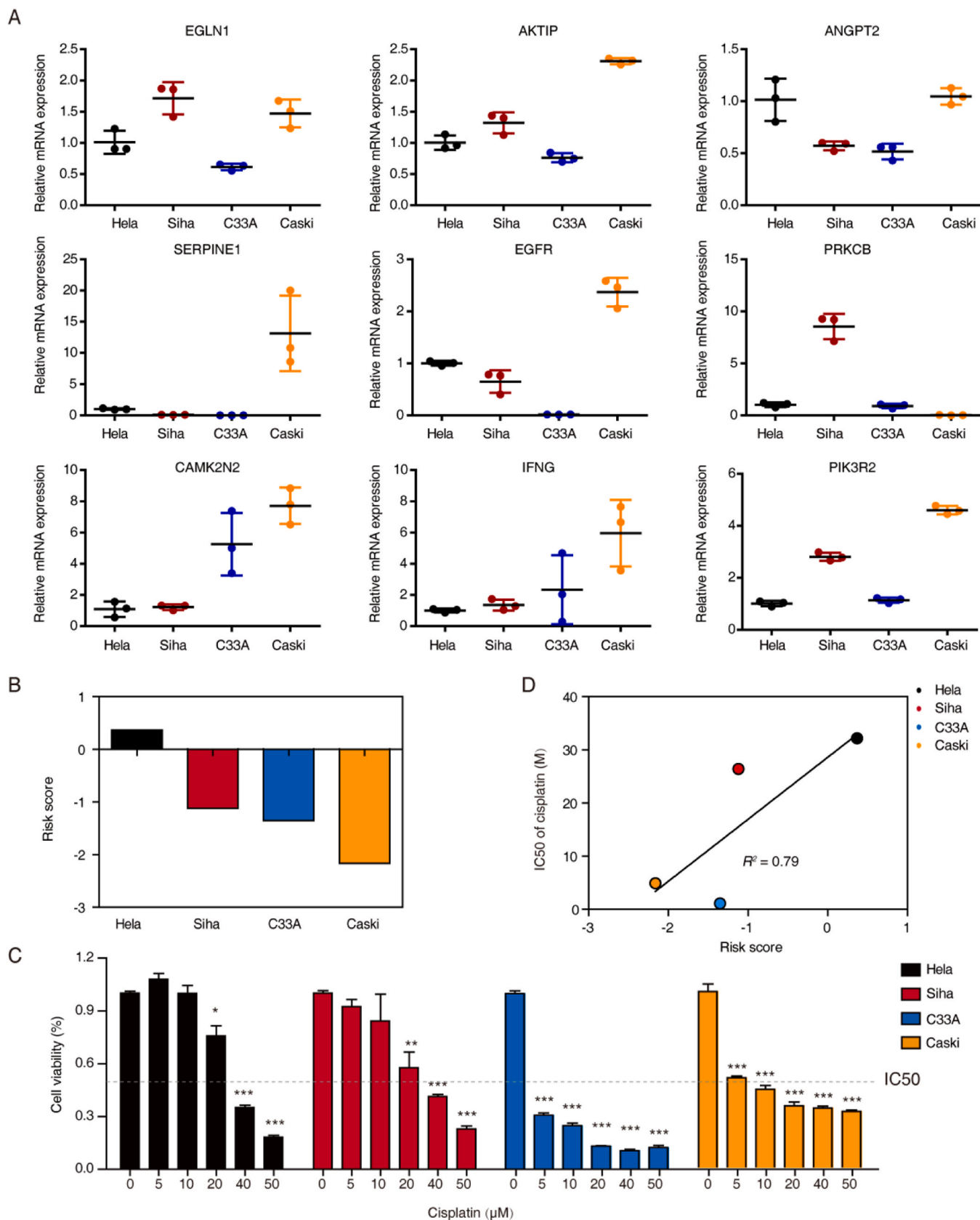
Fig. 4. Validation of the predictive capability of HRRS in cervical cancer cells regarding their response to cisplatin. (A) qRT—PCR analysis of the mRNA expression of *EGLN1, AKTIP, ANGPT2, SERPINE1, EGFR, PRKCB, CAMK2N2, IFNG*, and *PIK3R2* in four cervical cancer cell lines. (B) Risk score of the indicated cervical cancer cell lines calculated based on the HRRS formula. (C) Cell viability of cervical cancer cell lines treated with elevated concentrations of cisplatin (0–50 μM) for 24 h, as determined *via* CCK-8 assays. The bars indicate the SDs, n = 3; * $p < 0.05$, * * $p < 0.01$, * * * $p < 0.001$. (D) Correlation between the IC50 and risk score in the four cervical cancer cell lines.
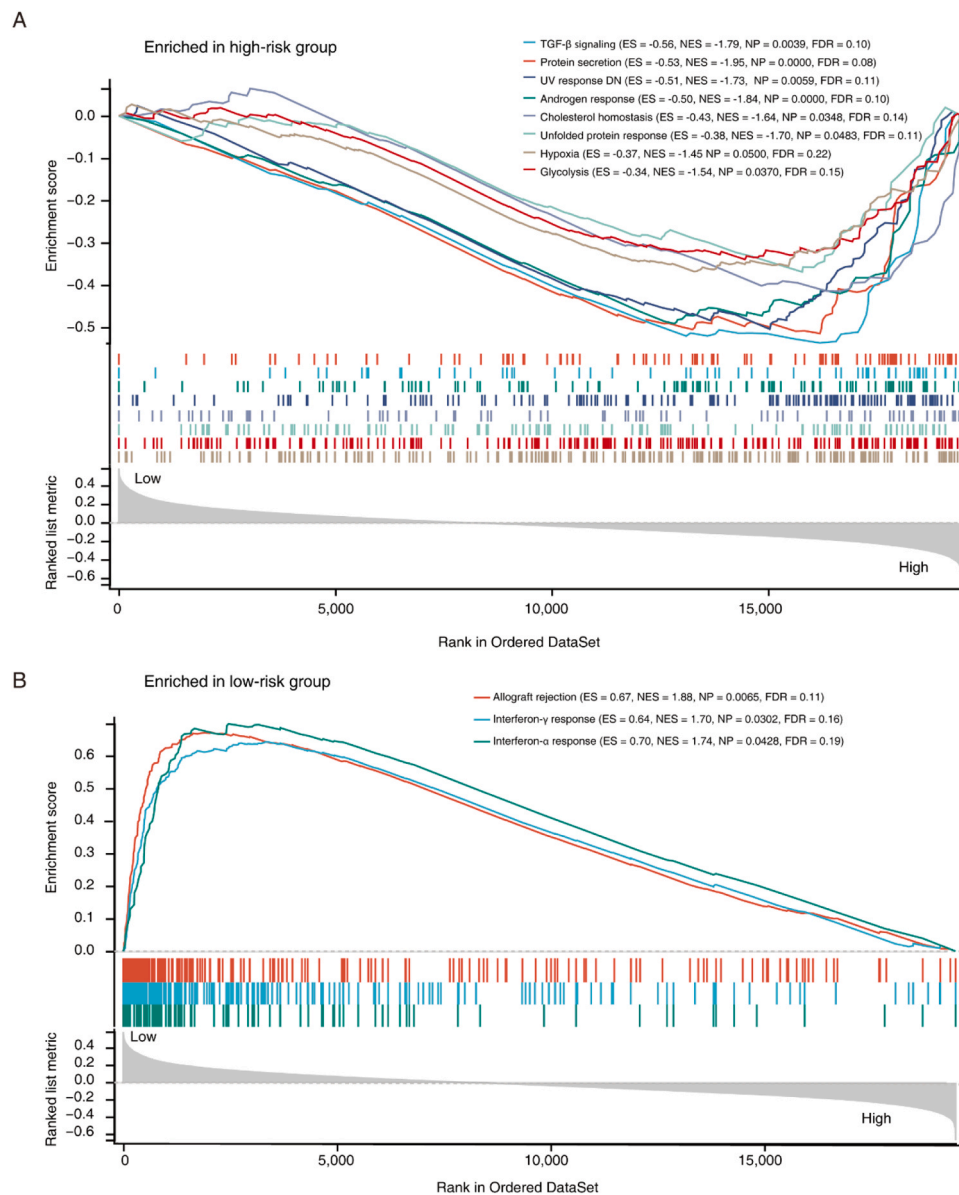
Fig. 5. Comprehensive analysis comparing hallmark gene sets in the high- and low-risk groups based on the HRRS. (A) Significant enrichment of hypoxia-related pathways and cancer proliferation-related pathways in high-risk patients with cervical cancer, as indicated by GSEA. (B) Significant enrichment of interferon response-related pathways in low-risk patients with cervical cancer, as indicated by GSEA.

sensitive cell lines C33A and Caski appeared to be more resistance to fostamatinib than did the cisplatin-resistant cell lines, with IC50 values of 35.94 ± 10.47 μM and 21.52 ± 4.89 μM, respectively (Fig. S3C), the fostamatinib-resistant effect in C33A and Caski cells was further confirmed by colony formation assay (Fig. S3D).

We next established a HeLa xenograft model to examine the anti-cancer effect of fostamatinib *in vivo*. Mice intraperitoneally injected with either 40 mg/kg or 80 mg/kg of fostamatinib exhibited significant inhibition of tumor growth. The inhibitory effect of fostamatinib on tumor growth increased along with the elevated concentration of fostamatinib, as evidenced by the reduced tumor volume observed in both 9.4 T MRI images (Fig. 8A) and the images of the excised HeLa tumors (Fig. 8B). Tumor growth curves (Fig. 8C), tumor weight (Fig. 8D) and Ki-67 proliferation index (Fig. 8E) further confirmed the efficacy of fostamatinib in inhibiting tumor growth. Moreover, TUNEL staining demonstrated a significant induction of tumor cell apoptosis following fostamatinib treatment compared to control group (Fig. 8F). Notably, evaluations of body weight, blood parameters, and histological examination of vital

organs (liver, kidney, spleen, lung, and heart) revealed no significant differences between the groups treated with various concentrations of fostamatinib and the control group (Fig. 8G-I). These findings suggest that fostamatinib treatment exerts a potent anticancer effect against cervical cancer with minimal adverse effects.

4. Discussion

Cisplatin-based chemotherapy is commonly employed for the treatment of various tumors, including cervical cancer. However, numerous patients develop resistance to cisplatin during treatment, thus leading to therapy failure and increased mortality rates [5]. Mounting evidence suggests that the hypoxic microenvironment fundamentally shields tumor cells against cisplatin treatment [7]. HIF-1, an oxygen-sensitive transcriptional activator, plays a crucial role in activating numerous genes that facilitate adaptation to hypoxia, including those that promote angiogenesis, cell survival, and drug resistance [46,47]. In this study, we constructed a HIF-1-related gene signature to suggest the clinical
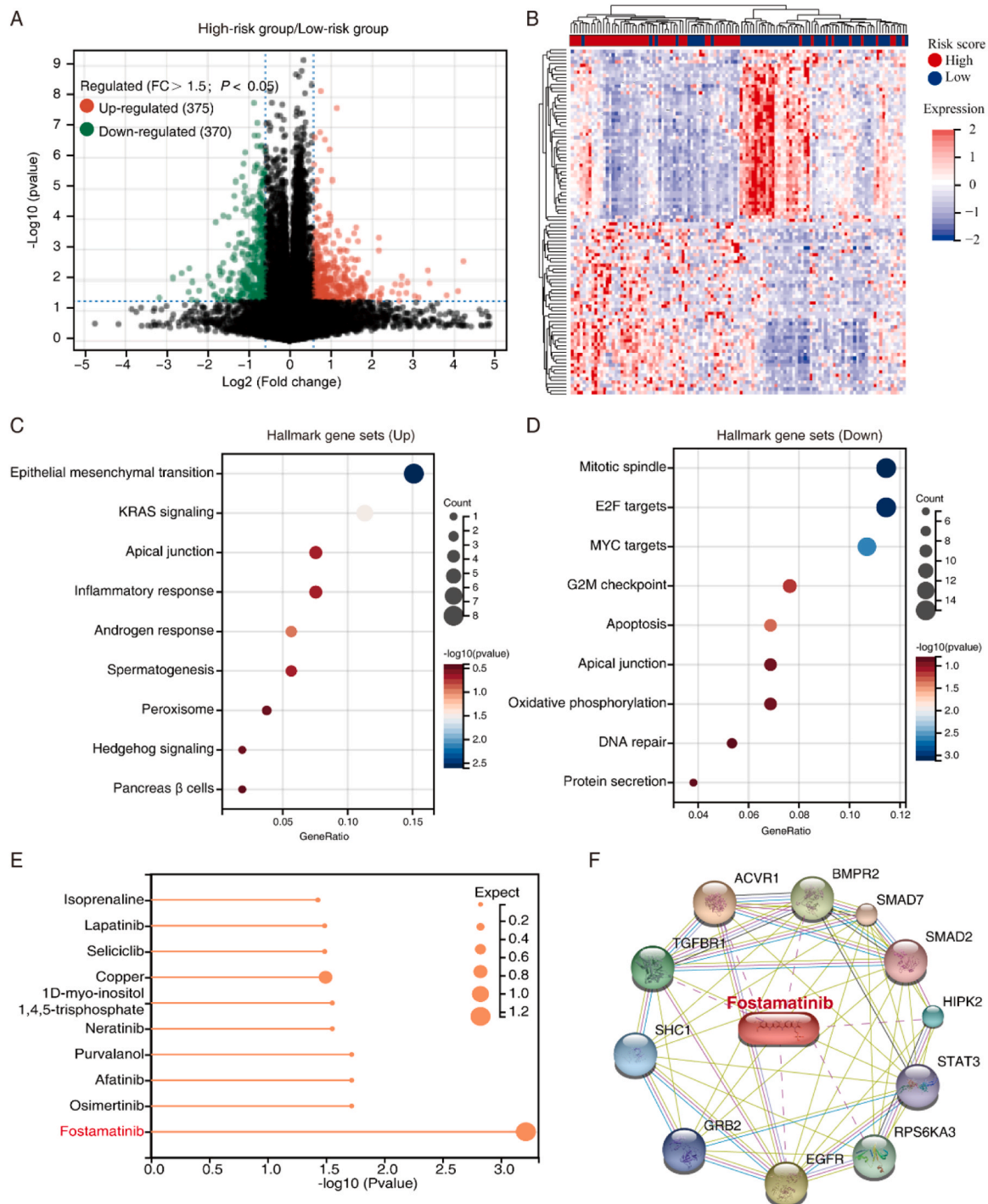
Fig. 6. Fostamatinib has potential efficacy against cervical cancer in high-risk groups. (A) Volcano plot of DEGs between the high- and low-risk groups: red points represent upregulated genes, black points indicate no significant change, and green points represent downregulated genes. (B) A heatmap depicting the top 50 up- and downregulated genes alongside their respective risk scores. (C) GSEA of upregulated genes to enrich hallmark gene sets. (D) GSEA of downregulated genes to enrich hallmark gene sets. (E) The WebGestalt web-based tool was used to predict drugs targeting the identified hallmark gene sets. (F) A gene–drug association network of fostamatinib and its associated genes.

outcomes and responses to cisplatin treatment in patients with cervical cancer. Moreover, we found that fostamatinib could benefit patients with cisplatin-resistant cervical cancer and validated its efficacy in inhibiting cervical cancer both *in vitro* and *in vivo*. Our study presents an effective method for suggesting cisplatin treatment outcomes prediction in patients with cervical cancer and provides a potential therapeutic strategy for patients with cervical cancer who exhibit tolerance to cisplatin.

Several hypoxia-based methods have been leveraged to assess clinical outcomes and therapeutic responses in patients with cancer, including pancreatic ductal adenocarcinoma [48] lung adenocarcinoma [15], hepatocellular carcinoma[48]. In this study, we focused on the influence of hypoxia on the clinical outcomes of cisplatin-treated patients with cervical cancer. To this end, we developed an HRRS prognostic model based on nine prognostic genes in the HIF-1 signaling pathway. Among the nine genes, five (*EGLN1, AKTIP, ANGPT2,*
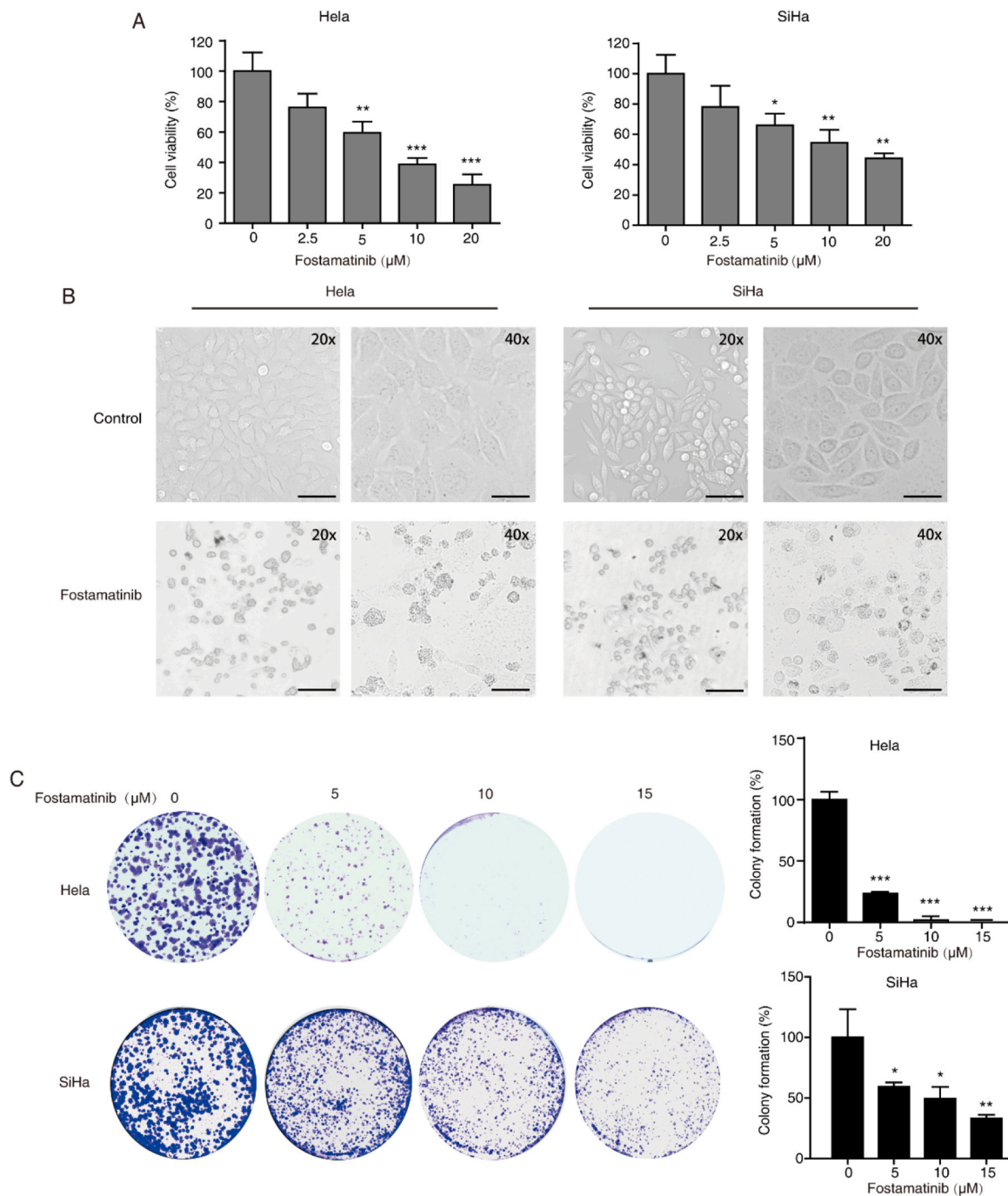
Fig. 7. Fostamatinib suppresses the growth of cervical cancer cells *in vitro*. (A) A CCK-8 assay was performed to assess the cell viability of HeLa and SiHa cells following treatment with increasing concentrations of fostamatinib (0–20 μM) for 24 h. (B) The morphology of HeLa and SiHa cells was examined after 24 h of incubation with fostamatinib (10 μM) or DMSO. Scale bar, 40 μm and 20 μm. (C) The colony formation ability of Hela and SiHa cells was compared after incubation with various concentrations of fostamatinib (0–15 μM). The bars indicate the SDs, n = 3; * $p < 0.05$, * * $p < 0.01$, * ** $p < 0.001$.

SERPINE1, and *EGFR*) were positively correlated with HIF-1 and considered to be risk factors, while the remaining four genes (*PRKCB*, *CAMK2N2*, *IFNG*, and *PIK3R2*) were negatively correlated with *HIF-1* and regarded as being protective factors.

To date, several studies have established their multigene models to predicts the prognosis of cervical cancer patients. A study developed a 15-gene classifier using generalized linear regressions and binomial logistic models, and demonstrated that the classifier could accurately identify patients with cervical cancer who would benefit from neo-adjuvant chemotherapy [49]. Moreover, a seven-gene signature (*ACSL1*, *ALDOA*, *FOXK2*, *GPI*, *MDH1B*, *MDH2*, and *MTHFD1*) associated with the TCA cycle [21] and a six-gene signature (*HSPA5*, *ANGPTL4*, *PFKM*, *GOT1*, *IER3*, and *PFKFB4*) associated with glycolysis [22] were developed to predict the prognosis of cervical cancer patients. However, gene models for predicting the prognosis of cisplatin-treated patients with cervical cancer remain limited. After side by side comparing their performance with our HRRS model based on cisplatin-treated patients (TCGA cohort), we found that, classified by the six-gene signature, cisplatin-treated patients with high-risk group displayed lower survival (HR = 2.85, $p = 3.8e\text{-}3$) than low-risk group, even so, our HRRS achieved greater sensitivity and specificity than other reported models in predicting the prognosis of patients with cervical cancer, and thus we
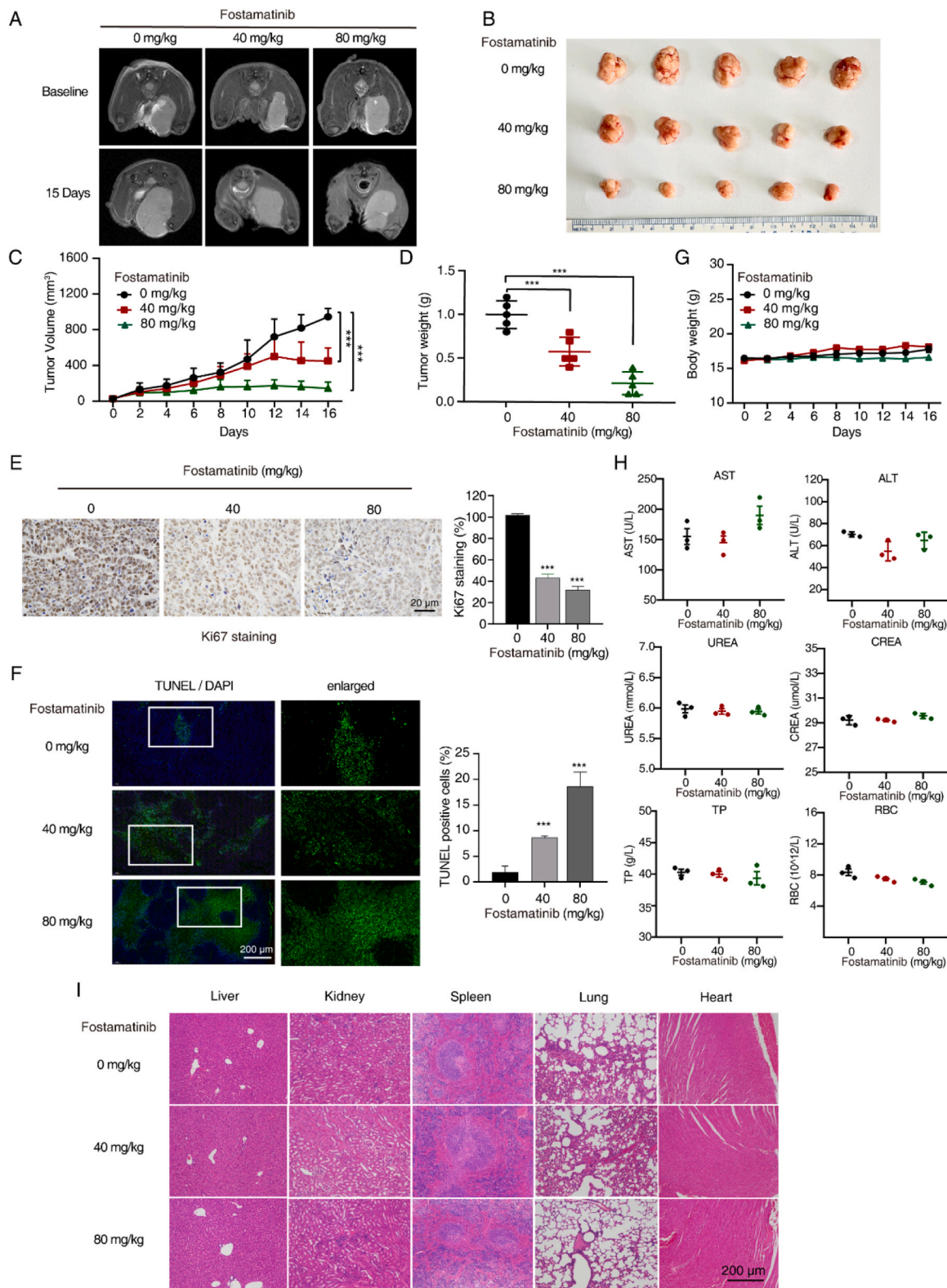
Fig. 8. Fostamatinib suppresses the growth of HeLa cell tumors *in vivo*. Nude mice bearing HeLa-derived xenografts were intraperitoneally injected with either fostamatinib (40 mg/kg or 80 mg/kg) or vehicle every other day (n = 5/group). (A) Tumor sizes were determined through MRI before and after treatment. (B) Representative tumors retrieved from xenograft models. (C) Tumor growth curves were generated for both the treatment and control groups. (D) Tumor weights in all three groups. (E) The Ki-67 proliferation index in tumor xenografts treated with fostamatinib or vehicle was analyzed *via* immunohistochemistry; Scale bar, 20 μm. (F) TUNEL assay of apoptotic cells in tissues. Blue corresponds to 4',6-diamidino-2-phenylindole (DAPI, nucleus), and green denotes TUNEL. Scale bar, 200 μm. (G) Mouse body weights were recorded every 2 days throughout the treatment period. (H) –Hematological parameters, including aspartate aminotransferase (AST), alanine aminotransferase (ALT), urea, creatinine (CREA), total protein (TP), and red blood cells (RBCs), were assessed in the specified groups. (I) Representative images of H&E staining of livers, kidneys, spleens, lungs, and hearts collected from the indicated groups. Scale bar, 200 μm. The bars indicate the SDs; * ** $p < 0.001$.

proposed the use of the HRRS as a potential individual factor for risk assessment and the determination of survival probability in cisplatin-treated patients.

In the TCGA cohort of patients with cisplatin-treated cervical cancer, the overall survival of patients with HRRS-high was negatively associated with a good prognosis. The general applicability of the HRRS model was validated using cervical cancer cell lines, which demonstrated that cervical cancer cell lines exhibiting low HRRS were significantly sensitive to cisplatin compared to those with high HRRS. This indicates that the HRRS is proficient in predicting the therapeutic efficacy of cisplatin in patients with cervical cancer. Our GSEA provided a partial explanation for the substantive difference observed between the different risk groups. We discovered that genes in the high-risk group were associated with several signaling pathways that contribute to chemoresistance and malignant tumor progression, such as EMT, TGF-β signaling, and glycolysis [38,50–52]. Conversely, upregulated genes in the low-risk group were significantly enriched in signaling pathways such as the interferon response [53] and apoptosis pathways, thus suggesting potential therapeutic options for cancer. These findings elucidate how disparate patterns of hallmark gene sets delineate the differences between the two HRRS groups in the cisplatin-treated TCGA cervical cancer cohort.

Fostamatinib, also known as R788, stands as the foremost approved specific SYK inhibitor for refractory immune thrombocytopenia [54]. SYK is a pivotal tyrosine kinase that induces BCR signaling to activate Ca^{2+} and PI3K signaling pathways [54], thereby emerging as a target for numerous diseases, including various immune system diseases and cancers [55]. As an effective SYK inhibitor, fostamatinib has considerable potential in cancer therapy. For example, fostamatinib has been reported to inhibit B-cell receptor signaling and cancer proliferation in chronic lymphocytic leukemia [44]. Additionally, recent studies have highlighted its ability to reprogram the tumor immune microenvironment, thus rendering it a potential treatment strategy for pancreatic ductal adenocarcinoma [45]. However, fostamatinib has not been utilized for cervical cancer treatment. Our bioinformatics analysis indicated that fostamatinib may be a potential therapeutic option for patients with cisplatin-resistant cervical cancer. Drug repurposing is an efficacious strategy for harnessing new applications of existing drugs beyond their original indications, with significant advantages in terms of cost savings and bypassing safety concerns [56]. Given the demonstrated feasibility of utilizing fostamatinib as an anticancer agent across various tumor types, repurposing it for treating cisplatin-resistant tumors has emerged as being a viable strategy.

Our analysis revealed that *EGFR, RPS6KA3, STAT3, HIPK2, SMAD2, SMAD7, BMPR2, ACVR1, TGFBR1, SHC1,* and *GRB2* as being primary targets of fostamatinib (Fig. 6F). Most of these genes are associated with EMT, immune response, and hypoxia. For example, *EGFR*, an epidermal growth factor receptor, plays a role in coordinating hypoxia-induced resistance and the development of EMT [57]. *STAT3*, initially identified as an IL-6 transcription factor, mediates hypoxia-induced gene expression and promotes EMT [58,59]. Therefore, targeting these genes in patients with cisplatin-resistant cervical cancer may modulate hypoxia, EMT, and immune crosstalk, thereby exerting significant anticancer effects. Our *in vivo* and *in vitro* experiments indicated that fostamatinib specifically suppressed those high-HRRS cervical cancer cells, underscoring its potential for treating cisplatin-resistant cervical cancer.

Certain limitations must be acknowledged in this study. First, the HRRS signature was developed using retrospective data obtained from the TCGA database, thus necessitating further validation with larger sample sizes in subsequent investigations. Second, *in vivo* and *in vitro* investigations are imperative to examine the role of the nine genes in cisplatin resistance in cervical cancer. Third, additional clinical samples and trials are necessary to substantiate the potential of fostamatinib for treating cisplatin-resistant cervical cancer.

5. Conclusion

We established HRRS as a tool to suggest clinical outcomes and therapeutic responses to cisplatin in patients with cervical cancer. Additionally, we discovered that fostamatinib, an FDA-approved SYK inhibitor, is a viable precision treatment for patients with cisplatin-resistant cervical cancer and high HRRS. Our findings hold significant promise for future therapeutic strategies.

CRediT authorship contribution statement

Weixiao Liu: Validation, Methodology, Investigation. **Yang Wang:** Writing – review & editing, Writing – original draft, Visualization, Supervision, Conceptualization. **Shuixing Zhang:** Writing – review & editing, Supervision, Funding acquisition. **Xuewei Wu:** Validation, Supervision. **Wannan Wang:** Visualization, Validation, Supervision, Investigation. **Jin Fang:** Methodology, Formal analysis, Data curation. **Jing Zhang:** Writing – review & editing, Writing – original draft, Supervision, Project administration, Funding acquisition, Data curation, Conceptualization. **Chen Li:** Writing – review & editing, Visualization, Validation, Methodology, Formal analysis. **Ying Wang:** Validation, Software, Methodology.

Declaration of Competing Interest

The authors declare that they have no known competing financial interests or personal relationships that could have appeared to influence the work reported in this paper.

Data availability

All data and materials are available from the corresponding authors upon request.

Appendix A. Supporting information

Supplementary data associated with this article can be found in the online version at doi:10.1016/j.csbj.2024.06.007.

References

[1] Siegel RL, Miller KD, Fuchs HE, Jemal A. Cancer Statistics, 2021. CA Cancer J Clin 2021;71:7–33.
[2] Liu C, Zhang M, Yan X, Ni Y, Gong Y, Wang C, Zhang X, Wan L, Yang H, Ge C, Li Y, Zou W, Huang R, Li X, Sun B, Liu B, Yue J, Yu J. Single-cell dissection of cellular and molecular features underlying human cervical squamous cell carcinoma initiation and progression. Sci Adv 2023;9. eadd8977.
[3] Abu-Rustum NR, Yashar CM, Bean S, Bradley K, Campos SM, Chon HS, Chu C, Cohn D, Crispens MA, Damast S, Fisher CM, Frederick P, Gaffney DK, Giuntoli R, Han E, Huh WK, Lurain Iii JR, Mariani A, Mutch D, Nagel C, Nekhlyudov L,

Fader AN, Remmenga SW, Reynolds RK, Sisodia R, Tillmanns T, Ueda S, Urban R, Wyse E, McMillian NR, Motter AD. NCCN Guidelines Insights: Cervical Cancer, Version 1.2020. J Natl Compr Canc Netw 2020;18:660–6.

[4] Cohen PA, Jhingran A, Oaknin A, Denny L. Cervical cancer. Lancet 2019;393: 169–82.

[5] Bhattacharjee R, Dey T, Kumar L, Kar S, Sarkar R, Ghorai M, Malik S, Jha NK, Vellingiri B, Kesari KK, Perez de la Lastra JM, Dey A. Cellular landscaping of cisplatin resistance in cervical cancer. Biomed Pharm 2022;153:113345.

[6] Kopecka J, Salaroglio IC, Perez-Ruiz E, Sarmento-Ribeiro AB, Saponara S, De Las Rivas J, Riganti C. Hypoxia as a driver of resistance to immunotherapy. Drug Resist Update: Rev Comment Antimicrob Anticancer Chemother 2021;59:100787.

[7] Devarajan N, Manjunathan R, Ganesan SK. Tumor hypoxia: The major culprit behind cisplatin resistance in cancer patients. Crit Rev Oncol Hematol 2021;162: 103327.

[8] Li Y, Zhao L, Li XF. Hypoxia and the Tumor Microenvironment. Technol Cancer Res Treat 2021;20. 15330338211036304.

[9] Wu Q, You L, Nepovimova E, Heger Z, Wu W, Kuca K, Adam V. Hypoxia-inducible factors: master regulators of hypoxic tumor immune escape. J Hematol Oncol 2022;15:77.

[10] Jing X, Yang F, Shao C, Wei K, Xie M, Shen H, Shu Y. Role of hypoxia in cancer therapy by regulating the tumor microenvironment. Mol Cancer 2019;18:157.

[11] Wang D, Zhao C, Xu F, Zhang A, Jin M, Zhang K, Liu L, Hua Q, Zhao J, Liu J, Yang H, Huang G. Cisplatin-resistant NSCLC cells induced by hypoxia transmit resistance to sensitive cells through exosomal PKM2. Theranostics 2021;11: 2860–75.

[12] Bao MH, Wong CC. Hypoxia, metabolic reprogramming, and drug resistance in liver cancer. Cells 2021;10.

[13] Wang H, Zheng L. Construction of a hypoxia-derived gene model to predict the prognosis and therapeutic response of head and neck squamous cell carcinoma. Sci Rep 2022;12:13538.

[14] Chen M, Chen Z, Lin Z, Ding X, Liang T. Utilization of hypoxia-derived gene signatures to predict clinical outcomes and immune checkpoint blockade therapy responses in prostate cancer. Front Genet 2022;13:922074.

[15] Shi R, Bao X, Unger K, Sun J, Lu S, Manapov F, Wang X, Belka C, Li M. Identification and validation of hypoxia-derived gene signatures to predict clinical outcomes and therapeutic responses in stage I lung adenocarcinoma patients. Theranostics 2021;11:5061–76.

[16] Regan-Fendt K, Li D, Reyes R, Yu L, Wani NA, Hu P, Jacob ST, Ghoshal K, Payne PRO, Motiwala T. Transcriptomics-based drug repurposing approach identifies novel drugs against sorafenib-resistant hepatocellular carcinoma. Cancers (Basel) 2020;12.

[17] T. Therneau, A Package for Survival Analysis in R. version 3.1–7, R Package, (2020).

[18] Therneau TM, Grambsch PM. The Cox Model. In: Therneau TM, Grambsch PM, editors. Modeling Survival Data: Extending the Cox Model. New York, NY: Springer New York; 2000. p. 39–77.

[19] Friedman J, Hastie T, Tibshirani R. Regularization paths for generalized linear models via coordinate descent. J Stat Softw 2010;33:1–22.

[20] Engebretsen S, Bohlin J. Statistical predictions with glmnet. Clin Epigenetics 2019; 11:123.

[21] Chen G, Hong X, He W, Ou L, Chen B, Zhong W, Lin Y, Luo X. The construction and analysis of tricarboxylic acid cycle related prognostic model for cervical cancer. Front Genet 2023;14:1092276.

[22] Cai L, Hu C, Yu S, Liu L, Yu X, Chen J, Liu X, Lin F, Zhang C, Li W, Yan X. Identification and validation of a six-gene signature associated with glycolysis to predict the prognosis of patients with cervical cancer. BMC Cancer 2020;20:1133.

[23] C. The Gene Ontology. The gene ontology resource: 20 years and still going strong. Nucleic Acids Res 2019;47:D330–8.

[24] Yu G, Wang LG, Han Y, He QY. clusterProfiler: an R package for comparing biological themes among gene clusters. OMICS 2012;16:284–7.

[25] Wu T, Hu E, Xu S, Chen M, Guo P, Dai Z, Feng T, Zhou L, Tang W, Zhan L, Fu X, Liu S, Bo X, Yu G. clusterProfiler 4.0: a universal enrichment tool for interpreting omics data. Innov (Camb) 2021;2:100141.

[26] Kanehisa M, Furumichi M, Tanabe M, Sato Y, Morishima K. KEGG: new perspectives on genomes, pathways, diseases and drugs. Nucleic Acids Res 2017; 45:D353–61.

[27] Subramanian A, Tamayo P, Mootha VK, Mukherjee S, Ebert BL, Gillette MA, Paulovich A, Pomeroy SL, Golub TR, Lander ES, Mesirov JP. Gene set enrichment analysis: a knowledge-based approach for interpreting genome-wide expression profiles. Proc Natl Acad Sci USA 2005;102:15545–50.

[28] Huang Z, Zhu S, Han Z, Li C, Liang J, Wang Y, Zhang S, Zhang J. Proteome-Wide Analysis Reveals TFEB targets for establishment of a prognostic signature to predict clinical outcomes of colorectal cancer. Cancers 2023;15.

[29] Zhang J, Zhou Y, Li N, Liu WT, Liang JZ, Sun Y, Zhang WX, Fang RD, Huang SL, Sun ZH, Wang Y, He QY. Curcumol Overcomes TRAIL Resistance of Non-Small Cell Lung Cancer by Targeting NRH:Quinone Oxidoreductase 2 (NQO2). Adv Sci 2020; 7:2002306.

[30] Liang X-L, Ouyang L, Yu N-N, Sun Z-H, Gui Z-K, Niu Y-L, He Q-Y, Zhang J, Wang Y. Histone deacetylase inhibitor pracinostat suppresses colorectal cancer by inducing CDK5-Drp1 signaling-mediated peripheral mitofission. J Pharm Anal 2023.

[31] Majoros H, Borsos BN, Ujfaludi Z, Pahi ZG, Morocz M, Haracska L, Boros IM, Pankotai T. SerpinB10, a serine protease inhibitor, is implicated in uv-induced cellular response. Int J Mol Sci 2021;22.

[32] Zhong L, Liao D, Li J, Liu W, Wang J, Zeng C, Wang X, Cao Z, Zhang R, Li M, Jiang K, Zeng YX, Sui J, Kang T. Rab22a-NeoF1 fusion protein promotes

osteosarcoma lung metastasis through its secretion into exosomes. Signal Transduct Target Ther 2021;6:59.

[33] Chen HY, Chan SJ, Liu X, Wei AC, Jian RI, Huang KW, Lang YD, Shih JH, Liao CC, Luan CL, Kao YT, Chiang SY, Hsiao PW, Jou YS, Chen Y, Chen RH. Long noncoding RNA Smyca coactivates TGF-beta/Smad and Myc pathways to drive tumor progression. J Hematol Oncol 2022;15:85.

[34] Freeman MR, Solomon KR. Cholesterol and prostate cancer. J Cell Biochem 2004; 91:54–69.

[35] Madden E, Logue SE, Healy SJ, Manie S, Samali A. The role of the unfolded protein response in cancer progression: From oncogenesis to chemoresistance. Biol Cell 2019;111:1–17.

[36] Icard P, Shulman S, Farhat D, Steyaert JM, Alifano M, Lincet H. How the Warburg effect supports aggressiveness and drug resistance of cancer cells? Drug Resist Update: Rev Comment Antimicrob Anticancer Chemother 2018;38:1–11.

[37] Kwon D, Schafer JM, Song NJ, Kaneko S, Li A, Xiao T, Ma A, Allen C, Das K, Zhou L, Riesenberg B, Chang Y, Weltge P, Velegraki M, Oh DY, Fong L, Ma Q, Sundi D, Chung D, Li X, Li Z. Androgen conspires with the CD8(+) T cell exhaustion program and contributes to sex bias in cancer. Sci Immunol 2022;7. eabq2630.

[38] Erin N, Grahovac J, Brozovic A, Efferth T. Tumor microenvironment and epithelial mesenchymal transition as targets to overcome tumor multidrug resistance. Drug Resist Update: Rev Comment Antimicrob Anticancer Chemother 2020;53:100715.

[39] Jaromi L, Csongei V, Vesel M, Abdelwahab EMM, Soltani A, Torok Z, Smuk G, Sarosi V, Pongracz JE. KRAS and EGFR Mutations Differentially Alter ABC Drug Transporter Expression in Cisplatin-Resistant Non-Small Cell Lung Cancer. Int J Mol Sci 2021;22.

[40] Ryan SL, Beard S, Barr MP, Umezawa K, Heavey S, Godwin P, Gray SG, Cormican D, Finn SP, Gately KA, Davies AM, Thompson EW, Richard DJ, O'Byrne KJ, Adams MN, Baird AM. Targeting NF-kappaB-mediated inflammatory pathways in cisplatin-resistant NSCLC. Lung Cancer 2019;135:217–27.

[41] Seidl C, Panzitt K, Bertsch A, Brcic L, Schein S, Mack M, Leithner K, Prinz F, Olschewski H, Kornmueller K, Hrzenjak A. MicroRNA-182-5p regulates hedgehog signaling pathway and chemosensitivity of cisplatin-resistant lung adenocarcinoma cells via targeting GLI2. Cancer Lett 2020;469:266–76.

[42] Everhov AH, Floter Radestad A, Nyberg T, Smedby KE, Bergmark K. A. Linden Hirschberg, Serum Androgen Levels and Sexual Function Before and One Year After Treatment of Uterine Cervical Cancer: A Pilot Study. J Sex Med 2016;13: 413–24.

[43] Fan Q, Huang T, Sun X, Yang X, Wang J, Liu Y, Ni T, Gu S, Li Y, Wang Y. miR-130a-3p promotes cell proliferation and invasion by targeting estrogen receptor alpha and androgen receptor in cervical cancer. Exp Ther Med 2021;21:414.

[44] Herman SE, Barr PM, McAuley EM, Liu D, Wiestner A, Friedberg JW. Fostamatinib inhibits B-cell receptor signaling, cellular activation and tumor proliferation in patients with relapsed and refractory chronic lymphocytic leukemia. Leukemia 2013;27:1769–73.

[45] Rohila D, Park IH, Pham TV, Weitz J, Hurtado de Mendoza T, Madheswaran S, Ishfaq M, Beaman C, Tapia E, Sun S, Patel J, Tamayo P, Lowy AM, Joshi S. Syk inhibition reprograms tumor-associated macrophages and overcomes gemcitabine-induced immunosuppression in pancreatic ductal adenocarcinoma. Cancer Res 2023.

[46] Infantino V, Santarsiero A, Convertini P, Todisco S, Iacobazzi V. Cancer Cell Metabolism in Hypoxia: Role of HIF-1 as Key Regulator and Therapeutic Target. Int J Mol Sci 2021;22.

[47] de Heer EC, Jalving M, Harris AL. HIFs, angiogenesis, and metabolism: elusive enemies in breast cancer. J Clin Invest 2020;130:5074–87.

[48] Chen D, Huang H, Zang L, Gao W, Zhu H, Yu X. Development and Verification of the Hypoxia- and Immune-Associated Prognostic Signature for Pancreatic Ductal Adenocarcinoma. Front Immunol 2021;12:728062.

[49] Tian X, Wang X, Cui Z, Liu J, Huang X, Shi C, Zhang M, Liu T, Du X, Li R, Huang L, Gong D, Tian R, Cao C, Jin P, Zeng Z, Pan G, Xia M, Zhang H, Luo B, Xie Y, Li X, Li T, Wu J, Zhang Q, Chen G, Hu Z. A Fifteen-Gene Classifier to Predict Neoadjuvant Chemotherapy Responses in Patients with Stage IB to IIB Squamous Cervical Cancer. Adv Sci 2021;8:2001978.

[50] Jeong H, Kim S, Hong BJ, Lee CJ, Kim YE, Bok S, Oh JM, Gwak SH, Yoo MY, Lee MS, Chung SJ, Defrene J, Tessier P, Pelletier M, Jeon H, Roh TY, Kim B, Kim KH, Ju JH, Kim S, Lee YJ, Kim DW, Kim IH, Kim HJ, Park JW, Lee YS, Lee JS, Cheon GJ, Weissman IL, Chung DH, Jeon YK, Ahn GO. Tumor-Associated Macrophages Enhance Tumor Hypoxia and Aerobic Glycolysis. Cancer Res 2019; 79:795–806.

[51] Taniguchi S, Elhance A, Van Duzer A, Kumar S, Leitenberger JJ, Oshimori N. Tumor-initiating cells establish an IL-33-TGF-beta niche signaling loop to promote cancer progression. Science 2020;369.

[52] Wang Y, Zhang J, Li YJ, Yu NN, Liu WT, Liang JZ, Xu WW, Sun ZH, Li B, He QY. MEST promotes lung cancer invasion and metastasis by interacting with VCP to activate NF-kappaB signaling. J Exp Clin Cancer Res: CR 2021;40:301.

[53] Borden EC. Interferons alpha and beta in cancer: therapeutic opportunities from new insights. Nat Rev Drug Discov 2019;18:219–34.

[54] Sadras T, Martin M, Kume K, Robinson ME, Saravanakumar S, Lenz G, Chen Z, Song JY, Siddiqi T, Oksa L, Knapp AM, Cutler J, Cosgun KN, Klemm L, Ecker V, Winchester J, Ghergus D, Soulas-Sprauel P, Kiefer F, Heisterkamp N, Pandey A, Ngo V, Wang L, Jumaa H, Buchner M, Ruland J, Chan WC, Meffre E, Martin T, Muschen M. Developmental partitioning of SYK and ZAP70 prevents autoimmunity and cancer. Mol Cell 2021;81:2094–111. e2099.

[55] Cooper N, Ghanima W, Hill QA, Nicolson PL, Markovtsov V, Kessler C. Recent advances in understanding spleen tyrosine kinase (SYK) in human biology and disease, with a focus on fostamatinib. Platelets 2023;34:2131751.

[56] Hu HF, Gao GB, He X, Li YY, Li YJ, Li B, Pan Y, Wang Y, He QY. Targeting ARF1-IQGAP1 interaction to suppress colorectal cancer metastasis and vemurafenib resistance. J Adv Res 2022.

[57] Saxena K, Jolly MK, Balamurugan K. Hypoxia, partial EMT and collective migration: Emerging culprits in metastasis. Transl Oncol 2020;13.

[58] Zhang X, Sai B, Wang F, Wang L, Wang Y, Zheng L, Li G, Tang J, Xiang J. Hypoxic BMSC-derived exosomal miRNAs promote metastasis of lung cancer cells via STAT3-induced EMT. Mol Cancer 2019;18:40.

[59] Bao Q, Zhang B, Suo Y, Liu C, Yang Q, Zhang K, Yuan M, Yuan M, Zhang Y, Li G. Intermittent hypoxia mediated by TSP1 dependent on STAT3 induces cardiac fibroblast activation and cardiac fibrosis. Elife 2020;9.